

# Bubble production by capillary-gravity waves

Ali R. Kolaini

National Center for Physical Acoustics, The University of Mississippi, University, Mississippi 38677

Lawrence A. Crum and Ronald A. Roy

Applied Physics Laboratory, University of Washington, Seattle, Washington 98105

(Received 23 March 1993; revised 22 September 1993; accepted 28 November 1993)

In the absence of whitecapping, other physical mechanisms may contribute to the generation of high-frequency ambient noise. It has been suggested [Longuet-Higgins, in *NATO Advanced Research Workshop on Sound Generation Mechanisms at the Open Surface* (NATO, Geneva, 1987)] that capillary waves, with surface profiles that are peaked downward in the troughs and are relatively flat at the crests, can inject acoustically active bubbles into the ocean, and thus contribute to the ambient noise background. It has been demonstrated in the laboratory that bubble injection can be generated at the trough of capillary-gravity, short-fetched waves by blowing air over water contained in a long, narrow tank. Simultaneous *in situ* acoustic and high-speed video monitoring of the capillary-gravity waves demonstrate that these waves can produce acoustically active bubbles. The generation of capillary waves depends principally upon the surface tension, which can be changed by adding surface-active agents to the water. The bubble production rate per unit area of these capillary-gravity waves was measured, as well as the dependence of this rate on wind speed, laboratory wind fetch, and surface tension. It was determined that an increase in water salinity and a reduction in surface tension increases the bubble production rate. The spectra of radiated frequencies ranges from 1 kHz to over 100 kHz with a broadband peak located around 4 kHz. The measured spectral densities were weakly related to wind speed. The wind-speed threshold value for bubble production was determined to be approximately 8.6 m/s (14.6 m/s at 10-m level) in fresh water and salt water, which decreased to 8.1 m/s (13.8 m/s at 10-m level) with a surface tension of 40.5 dyn/cm.

PACS numbers: 43.30.Lz, 43.30.Nb

## INTRODUCTION

It is generally recognized that breaking waves of various types is the dominant source of ambient noise in the ocean.<sup>1,2</sup> However, the production of ambient noise by capillary waves (with surface tension as a restoring force) or capillary-gravity waves (with surface tension and gravity as restoring forces) has only recently been mentioned in the literature<sup>3</sup> as a source of low wind speeds. Casual observation of a wind-wave field indicates that small capillary waves are present on the front face of longer gravity waves. Using a plunging-type wavemaker, Cox<sup>4</sup> conducted a series of experiments in which he was able to observe capillary waves riding on gravity waves in the absence of wind; furthermore, wind blowing in the same direction as wave propagation augmented the ripples. For steep gravity waves ( $5 \text{ cm} < \lambda < 50 \text{ cm}$ ) surface tension becomes important at the crest region and leads to traveling disturbances resulting in capillary wave production.<sup>5</sup>

In general, the dispersion relation for surface waves on deep water is given by (Lighthill<sup>6</sup>)

$$\omega^2 = (g + \tau k^2 / \rho) k, \quad (1)$$

where  $\omega$  is the angular frequency of oscillation,  $g$  is the acceleration due to gravity,  $\rho$  is the liquid density,  $k$  is the wavenumber, and  $\tau$  is the surface tension. For higher surface tensions, gravity becomes less important than the surface tension in the generation of these waves. The ratio of

these two forces can be defined by a dimensionless parameter  $\Delta$ ,

$$\Delta = 4\pi^2 \tau / \rho \lambda^2 g, \quad (2)$$

where  $\lambda$  is the wavelength. Neglecting gravity ( $\Delta \rightarrow \infty$ ), an exact solution to the nonlinear differential equation governing capillary wave propagation was given by Crapper.<sup>7</sup> Profiles for these nonlinear, purely capillary waves are shown in Fig. 1 for different steepness ratios,  $a/\lambda$ , where  $a$  is the wave height. Unlike trochoidal gravity waves, capillary waves possess relatively flat crests and sharp troughs. Crapper's calculations predict a limiting steepness ratio of approximately 0.73, at which point the surfaces of adjacent waves come in contact and trap air in trough regions. Beyond this limiting case Crapper's results become nonphysical because the sides of adjacent waves then pass through each other. Experiments performed by Schooley<sup>8</sup> confirmed his theory with short-fetch, wind-generated water waves. Two years later, Schooley<sup>9</sup> observed double, triple, and higher-order dimples riding on the front faces of gravity waves. The dimples were a few centimeters in wavelength, as was predicted by Wilton.<sup>10</sup>

The problem of two-dimensional, steady, nonlinear capillary-gravity waves has been considered by Hogan<sup>11-14</sup> and the role of surface tension on breaking gravity waves has been observed experimentally by Miller.<sup>15</sup> By adding chemicals to water, Miller was able to change the surface tension and measure the limiting steepness,  $a/\lambda$ , as well as

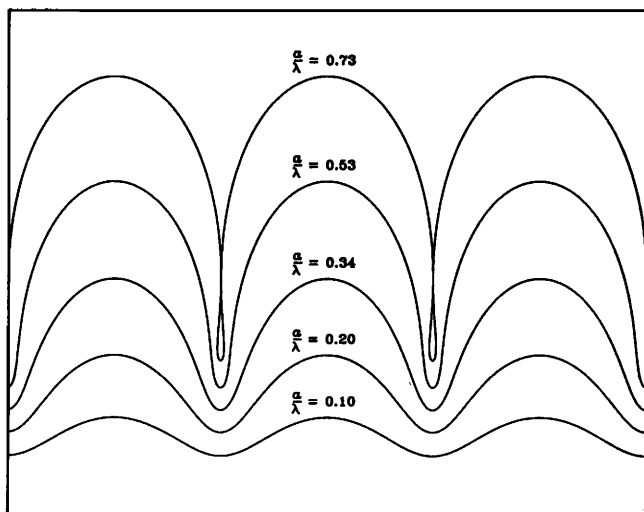


FIG. 1. Wave profiles of nonlinear capillary waves (after Crapper<sup>7</sup>).

the limiting wave angle. From this study, he concluded that as surface tension decreased, the amplitude of steady propagating gravity waves increased, while delaying the onset of the breaking wave. This result has been confirmed by recent theoretical work by Hogan of inviscid gravity-capillary waves.<sup>12</sup> It was evident by Hogan's calculations that a bubble could be encapsulated in the trough region of several limiting capillary-gravity wave profiles.

More recently, Updegraff and Anderson<sup>16-17</sup> investigated surface noise mechanisms from a depth of 1 m in the open ocean at low wind speeds. They showed that the wind-generated noise from the ocean surface at low wind speeds was caused by small spilling breakers and their acoustic measurements showed resemblance to the gentle spilling breakers produced in the laboratory by Medwin and Beaky.<sup>18</sup> Wilson<sup>19</sup> observed the ambient noise source level to be wind and whitecap dependent and concluded that three noise regimes existed—one prior to wave breaking, one after breaking with whitecap index, and one at wind speeds greater than 6 m/s in fully developed sea state conditions. Kerman<sup>20</sup> showed that the ambient noise spectral levels also depend on the wind speed and frequency and are consistent with the observations of Kundsen<sup>1</sup> and Wenz.<sup>2</sup>

The ambient noise level can be significantly reduced in the presence of a monomolecular film on the sea surface.<sup>21</sup> In some instances, maximum noise reductions of about 6 dB were observed at the low sea states beneath the monomolecular films.<sup>21,22</sup> These films had a pronounced quieting effect even when whitecaps were not present. Capillary waves can also be affected by films and have been reported to be attenuated by factors of about 2-4 in the presence of surface-active materials.<sup>23</sup>

The object of this paper is to demonstrate experimentally that bubbles can indeed be produced in the trough regions of capillary-gravity waves driven by a laboratory short-fetch wind generator and that these bubbles are acoustically active, and, thus, may contribute to the high-frequency ambient noise level in the ocean. Using a high-

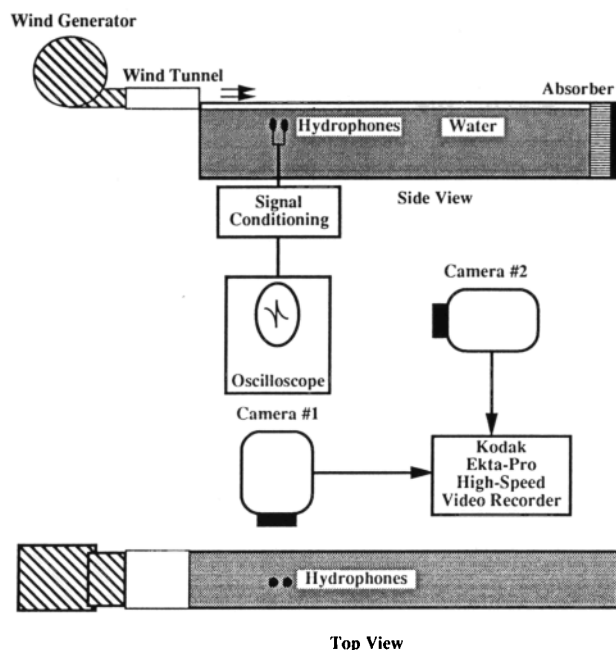


FIG. 2. Schematic drawing of the experimental arrangement.

speed video camera we were able to record the bubble entrapment by capillary waves and to correlate the acoustic emissions with the injection of these bubbles. In addition, bubble production rates and size distributions were measured using acoustic techniques. Observations and quantitative measurements were repeated for a variety of wind speeds, surface tensions, and laboratory fetches.

## I. EXPERIMENTAL PROCEDURES

Wind-driven capillary-gravity waves were produced in a 9 cm × 22 cm × 150 cm (width, height, length) Plexiglas tank. The tank was filled with distilled water to a depth of 21 cm. Wind was directed from left to right by means of a variable speed air blower and a wind tunnel that was 50 cm long and 10 cm × 20 cm in cross-sectional area (Fig. 2). The mean wind velocity was varied from about 8.40 to 16.20 m/s and was measured in the cross section of the wind tunnel at the entrance to the tank with a miniature Pitot tube. The traveling waves were absorbed by coarse fibrous material positioned at the opposite end of the tank and very few standing waves were observed. The distribution of wind speed, measured at the tank entrance, against the height above the still-water surface is illustrated in Fig. 3. The mean wind speeds, ranging from 8.40 to 16.2 m/s, were computed from these profiles and are used throughout this report. The wind speed at the tunnel exit is not the same as the wind speed at the points of bubble production, and it was determined to be inversely proportional to the fetch. The velocity profiles about 0.5 cm above the undisturbed water surface were represented approximately by the logarithmic law,  $u = u^* \kappa^{-1} \ln(z/z_0)$ , where  $u^* = \sqrt{\sigma_0/\rho}$ ,  $\kappa$  is Karman's universal turbulent constant,  $z_0$  is the effective roughness parameter,  $\sigma_0$  is the shear stress at the surface, and  $\rho$  is the air density. Even though the velocity profiles of the laboratory short-fetched waves obeyed the logarithmic law, direct scaling to ocean parameters

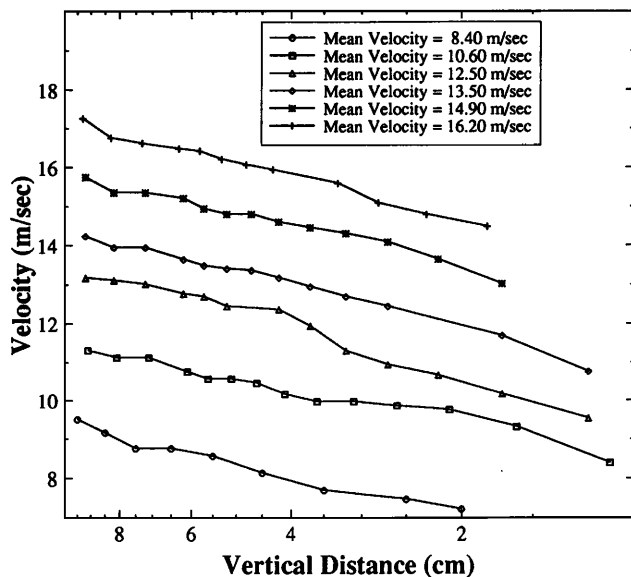
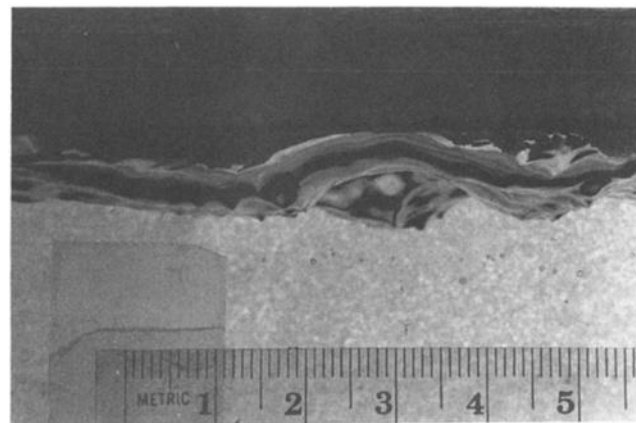


FIG. 3. Wind speed distribution for various mean velocities. These profiles were measured above the still water surface at the entrance to the tank and are represented approximately by the logarithmic law.

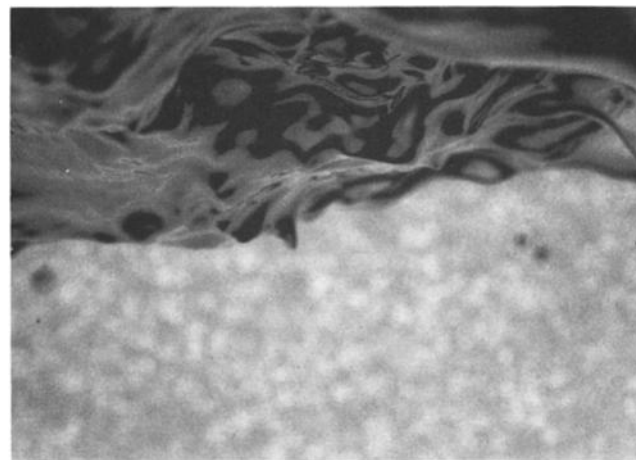
may not be possible. In order to scale laboratory wind-driven, capillary-gravity waves to the ocean waves, it is necessary to generate waves with longer fetches (Toba<sup>24</sup>). The wind-generated waves in our laboratory arrangement had fetches that were many orders of magnitude less than those at sea. However, the spectral form of the ocean surface waves in the capillary-gravity range has been found to be unaffected by the existence of large dominant waves in the gravity range and is independent of the fetch.<sup>25</sup>

Laboratory short-fetched capillary wave formation appeared when the average wind velocity at the entrance to the tank reached approximately 5.1 m/s (10 kn). Increasing the wind velocity increased the steepness of the capillary-gravity waves with capillary profiles riding in front of the gravity waves and possessing flat crests with sharp troughs. Still photographs of capillary-gravity waves with sharp troughs are shown in Fig. 4. Wavelengths of the gravity waves were estimated to be on the order of a few centimeters (ripples) while capillary wavelengths were on the order of few millimeters. Note that the capillary waves are not characterized by a single frequency and amplitude. This is due in part to the fact that the driving force of the wind is inherently broadband. These photographs show wavelets that have a profile that peaks downward, confirming Crapper's theory for capillary waves. As Crapper suggested for pure capillary waves, air bubbles are trapped at the troughs once the limiting condition is met. As the trough of a prominent capillary wave encapsulates air, it is often elongated as a result of local fluid particle motion, and the trapped air separates from the trough region.<sup>26</sup> The bubble that is produced is dynamically unstable and radiates energy by acoustic emissions.

Using two synchronized Kodak Ektapro high-speed video cameras, we recorded images of the activity along a 3-cm segment of the water surface (measured along the length of the channel) while *simultaneously* recording (via



(a)



(b)

FIG. 4. Photographs of capillary-gravity waves moving from left to right. Photo (a) is a broad view while (b) is a close-up of the 2-cm-long wave field. Profiles of capillary waves, peaked downward are clear.

an oscilloscope) the pressure measured by a submerged B&K 8103 broadband hydrophone with a plane wave sensitivity of  $-208.8$  dB *re*:  $1$  V/ $\mu$ Pa. The first camera employed a Nikon 108-mm lens directed perpendicular to the direction of wave propagation and was tilted slightly upward to visualize better the trough regions of the capillary waves. The second camera, which was equipped with a Nikon 48-mm lens, was focused on the display of the analog oscilloscope. Both cameras were synchronized and operated at 1000 frames/s. This allowed us to visualize the evolution of the bubble entrainment process and establish the causal relationship between bubble production and sound generation.

It is important to note that the small-tank visual records of bubble production encompassed a region of the surface only 3 cm long and 9 cm across, whereas the acoustical record could potentially include sound generated by bubbles throughout the *entire* channel. This makes it difficult to correlate unambiguously observed bubble production with specific acoustical signals. To alleviate this problem, we devised the system diagrammed in Fig. 5. Two B&K 8103 hydrophones were symmetrically positioned 8 cm apart as shown with the axis of symmetry correspond-

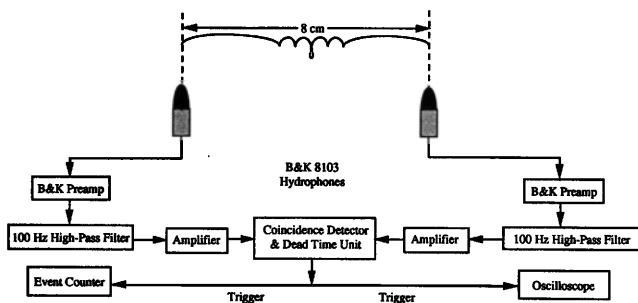


FIG. 5. Schematic of bubble entrapment by capillary waves and block diagram of bubble detection instrumentation.

ing to the center of the video camera's horizontal field of view. The preamplified and filtered outputs of both hydrophones were fed into a coincidence unit, which generated an output logic pulse contingent upon the "simultaneous" arrival of an acoustic signal at the two hydrophones. A coincident time of  $10 \mu\text{s}$  was chosen. The region in which signals generated by bubbles to be included by our coincidence criterion with  $10 \mu\text{s}$  duration time and a prespecified trigger level of the unit was mapped experimentally. To determine this region we artificially generated bubbles by releasing water drops from a hypodermic needle held above the water surface. The height of the needle was adjusted in such a way that a drop would generate an acoustically active bubble.<sup>27</sup> The bubble production region was mapped by moving the needle to new locations and monitoring the acoustic signal leaving the coincidence detector. Figure 6 shows our experimentally mapped region where the coincidence detector was able to receive acoustic signals for the aforementioned settings. The locations of two B&K hydrophones are also shown in this figure. The area where the coincidence unit was able to receive an acoustic signal independent of frequencies and amplitudes was approximately  $43 \text{ cm}^2$ . This area is identified by a shaded

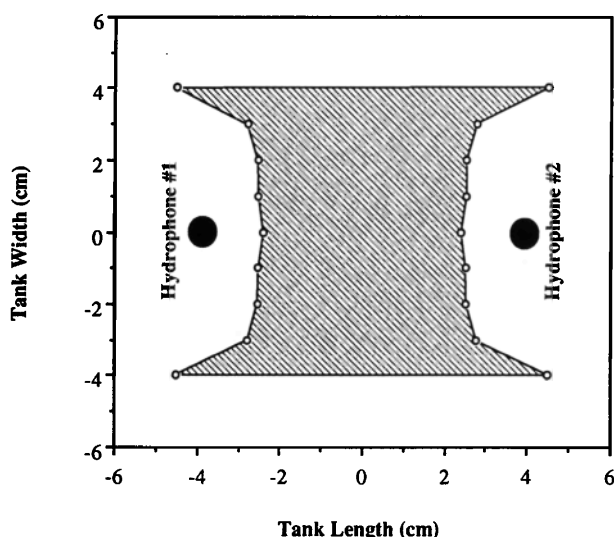


FIG. 6. Map of the region where the coincident detector can detect bubbles. Two B&K hydrophones were placed 8 cm apart and were located in the center of the tank.

region shown in Fig. 6 where open circle marks indicate the acoustic signal boundary identified by coincident detector.

Some problems arose with this technique: The fixed prespecified trigger level of the unit may have been higher than the pressure amplitude of the low-frequency bubbles at the end of  $10 \mu\text{s}$ . The slope of the acoustic signal of the low-frequency bubbles is much smaller than the high-frequency ones. This difference may have resulted in exclusion of low-frequency bubbles if the trigger level were set above their pressure amplitudes. To correct this problem, the outputs of the filters were fed into a high-gain stage, which saturated at the instant the pulse arrived and thus provided a frequency- and amplitude-independent arrival pulse, which was then fed into the coincidence unit. The output of the modified unit was fed into a counter (for bubble-counting purposes). This system allowed us to display or count only the acoustic signals produced by bubbles generated within a  $43\text{-cm}^2$  surface under acoustical observation. A dead time of 5 ms was incorporated into the system to avoid multiple counting due to lengthy acoustic signals or multiple reflections.

Prior to each experiment the water temperature and surface tension were, respectively, measured using a mercury thermometer and a DuNuoy ring tensiometer. The variations in the respective values by no more than  $\pm 1^\circ\text{C}$  and  $\pm 1.5 \text{ dyn/cm}$  from the mean temperature and surface tension were determined by periodic inspection. The mean temperature of water in the tank was approximately  $18^\circ\text{C}$ . The laboratory fetch was varied from 25 to 100 cm and the wind speed was varied from 8.4 to 16.2 m/s by adjusting the voltage delivered to the wind generator. The basic measurements included acoustical records of bubble generation as well as estimates of mean bubble production rates for a variety of wind speeds and surface tensions, the latter of which was varied by adding controlled quantities of ethyl alcohol as a surfactant. The effect of water salinity on bubble production rate was also examined by adding enough Instant Ocean Salt to the water to make its salinity comparable with the salinity of the ocean (33-g salt/1000-g water, surface tension 74 dyn/cm). We also transferred the wind generator to an anechoic tank ( $12 \times 12 \times 8 \text{ ft}$ ; width, length, height) and used a B&K 8105 Hydrophone to measure the power densities as a function of wind speed. Through these experiments, we sought to establish that capillary-gravity waves from acoustically active bubbles and to gain insight into how the generated bubble sizes and production rates scale with the length scales and energetics of the surface waves.

The dependence of average bubble-production rate on laboratory wind fetch (i.e., distance from the wind generator) was measured by moving the hydrophone holder away from the wind generator with a 15-cm increments using an automated system. The hydrophone support device was connected to a precision stepping motor via a rack and pinion gear. Using a Macintosh II computer, the stepping motor was able to move hydrophones accurately to new positions along the tank's length. The computer also enabled us to record automatically the output of the fre-

quency counter and then transfer these data to files. For each case, we measured production rates by counting detected acoustic emissions over a 25-min interval, from which we estimated a rate in bubbles/s. This was repeated five times and the mean rate calculated. The average value, standard deviation, and maximum/minimum of the bubble production rates were measured and saved on a disk. The water level in the tank was controlled by a level monitor attached at one end of the tank.

## II. RESULTS

### A. Air entrainment mechanism in capillary-gravity waves

Using high-speed video cameras, we were able to obtain visual records of bubbles entrained by elongated capillary wave troughs. Figure 7(a) shows photographs of a sequence of frames taken from the Kodak Ekta-Pro video system at a speed of 1000 frames/s. The dark region is the indicative of the surface of the capillary waves at trough regions. These images show the capillary-gravity waves propagating from right to left of the image. At the top right corner of the frame #1, air is contained within the trough region of the capillary wave (see the indicator); this trough is elongated by the particle velocity of the flow below the water surface (frames #1–3). Frames #4–6 show the elongated trough is truncated and a bubble is entrained. This bubble then breaks into at least two smaller bubbles. Figure 7(b) also shows a close-up of a sequence of digitized frames of capillary-gravity waves at high wind speed taken from the Kodak Ekta-Pro video system at the same rate as Fig. 7(a). In Fig. 7(b) two video cameras captured, simultaneously, the images of the capillary-gravity waves propagating from right to left of the image. The first camera recorded the image of capillary waves and the second one recorded the corresponding sequence of an oscilloscope, which was triggered from the output of the coincidence unit. At the left bottom corner of frame #1I, air is contained within the trough region of the capillary wave (see the indicator); this trough is deformed by the particle velocity of the flow below the water surface (frames #2I–3I). Frames #4I–5I show that the elongated trough is truncated and a bubble is entrained (see the indicator). The acoustic emissions from this entrained bubble are shown in frames #4II–5II. Numerous video records indicate the presence of a prominent acoustical signal at the instant that a bubble is entrained—clear evidence of the causal relationship between capillary wave bubble production and acoustic emission. Video observations also indicate that, in addition to the capillary wave gas entrainment mechanism described above, bubbles are also formed from gas entrained by very gentle spilling gravity waves. This latter process is more prominent at high wind speeds.

The pressure-time trace and power spectrum of a typical acoustic emission is given in Fig. 8. The signal was recorded on a LeCroy 9400 digital oscilloscope operating at a digitizing rate of 2.5 M samples/s and triggered by the output from the coincidence unit. In this instance, the wind

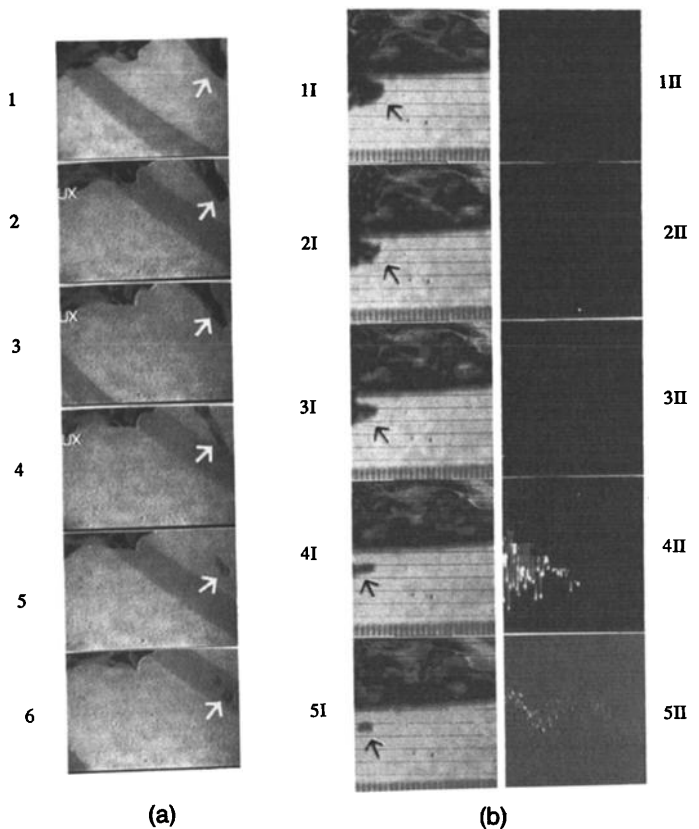


FIG. 7. (a) Photographs of a sequence of frames from high-speed video camera depicting the bubble entrapment and detachment from the trough region (frames 1–6). At the top corners of these images, shown with indicator, the trough region of the capillary waves have encapsulated the air. This trough is elongated by the particle velocity of the flow below the water surface. Frames #4–6 show that the elongated trough is truncated and a bubble is entrained which breaks into at least two smaller bubbles. These frames are sequential and are 2 ms apart. (b) Digitized images of a sequence of frames are also shown here. In this figure two cameras were used: one views bubble entrapment and the other captures images of an oscilloscope trace showing the simultaneous radiated acoustic pressure generated by the bubble. We have made use of the interleave mode where both images were simultaneously captured on separate frames. A bubble is pinched off in frame #4I shown by an indicator. The acoustic emissions from the bubble are shown in frames 4II and 5II. Frames in (b) are sequential and are 2 ms apart. The images shown in (a) and (b) of the capillary-gravity waves, moving from right to left, were made at a speed of 1000 frame/s.

speed was 13.5 m/s and the surface tension was 67 dyn/cm. The waveform resembles an exponentially decaying sinusoid, which is the classic acoustical signature of a bubble undergoing damped volume pulsations. The power spectrum [Fig. 8(b)] has a prominent peak at 3.2 kHz, which indicates a bubble diameter of roughly 2.05 mm; using the Minnaert formula<sup>28</sup> the bubble size can be calculated:

$$R = (1/2\pi f) \sqrt{3\gamma P_0/\rho}, \quad (3)$$

where  $R$  is the bubble radius,  $f$  is the resonance frequency,  $P_0$  is the ambient pressure,  $\gamma$  is the specific heat ratio equal to 1.4 for adiabatic processes, and  $\rho$  is the liquid density. Figure 9(a) depicts the emissions from several bubbles created sequentially with a wind speed of 14.9 m/s and a surface tension of 67 dyn/cm. The center frequencies of

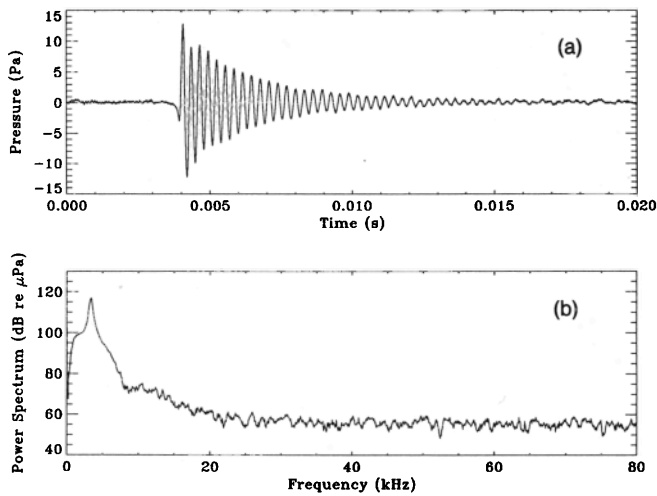


FIG. 8. Pressure traces and power spectrum of acoustic emission from capillary-gravity waves; wind speed=13.5 m/s, surface tension=67.0 dyn/cm. The bubble diameter is approximately equal to 2.05 mm.

some of these emissions are 5.0, 5.8, and 13.0 kHz as shown in Fig. 9(b), which correspond to bubble diameters of approximately 1.31, 1.13, and 0.50 mm, respectively. Finally, in Fig. 10, we observe two distinct bubbles at 38 and 66.5 kHz (diameter  $\approx$  172.5 and 98.6  $\mu$ m). These data serve to illustrate the broad range of emitted frequencies as well as the high bubble production rates attainable from wind-driven capillary-gravity waves.

## B. Ambient noise spectra

The accurate measurement of the spectral characteristics of discrete, broadband acoustic emissions requires an enclosure, devoid of multipaths and reverberation, a condition that is certainly not supported by the narrow tank illustrated in Fig. 2. To alleviate this problem, we mounted the wind generator at one end of the larger anechoic tank (12 $\times$ 12 $\times$ 8 ft) and submerged the hydrophone about 13 cm beneath the still-water line and 70 cm from the gener-

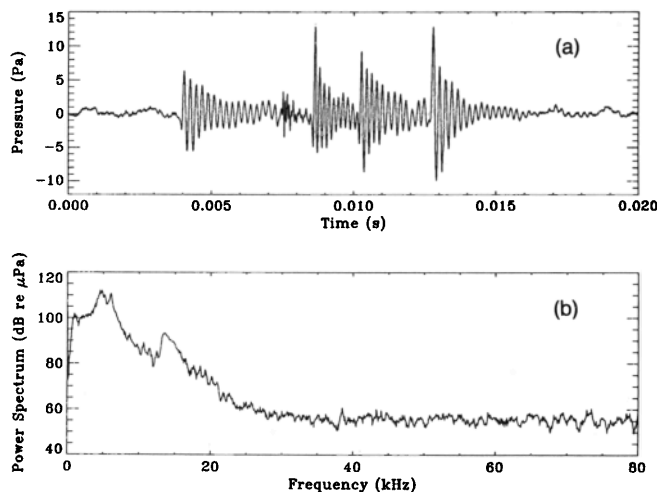


FIG. 9. Pressure trace and power spectrum of acoustic emissions from capillary-gravity waves; wind speed=14.9 m/s, surface tension=67.0 dyn/cm. The bubble diameters are 1.31, 1.13, and 0.50 mm, respectively.

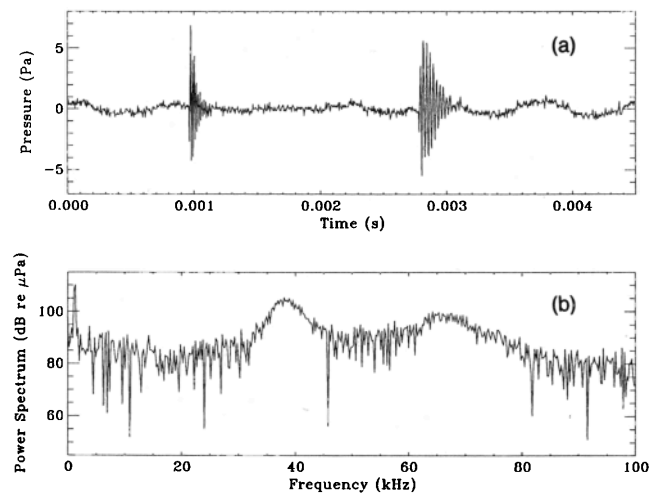


FIG. 10. Pressure trace and power spectrum of acoustic emission from capillary-gravity waves; wind speed=16.2 m/s, surface tension=67.0 dyn/cm. The bubble diameters are 172.5 and 98.6  $\mu$ m, respectively.

ator. The surface wave fronts of the capillary-gravity waves produced in this tank were circular as opposed to the planar waves produced in the small tank. However, the influence of circular waves *vis à vis* planar waves on the measured acoustic power spectrum was not investigated.

The bubble size distributions of the capillary-gravity waves were measured by continuously recording the acoustic signals of bubbles for five minutes in the anechoic tank. The individual resonance frequencies of bubbles were calculated from discrete bubble events and the sizes of the bubbles were calculated using Eq. (3). Figure 11(a)–(d) shows four histograms of capillary-gravity bubble production rates for mean wind speeds of 12.5, 13.5, 14.9, and

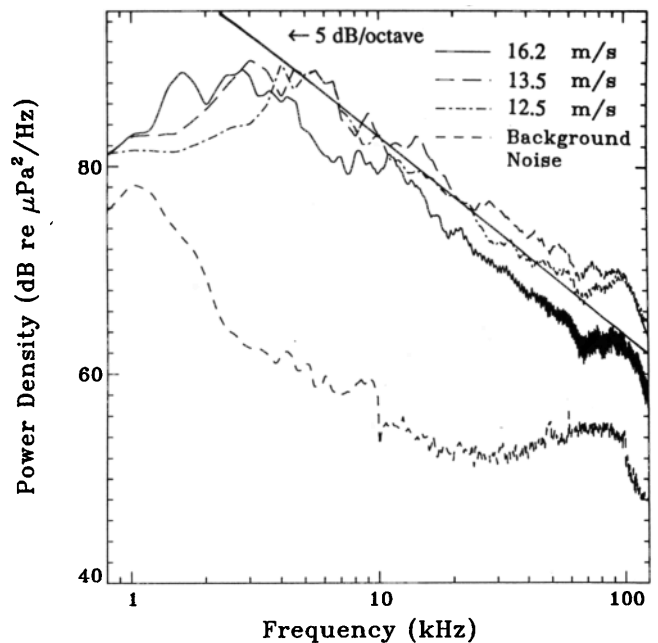


FIG. 11. Histogram of bubble production rate per minute for four different wind speeds: (a) 12.5 m/s, (b) 13.5 m/s, (c) 14.9 m/s, and (d) 16.2 m/s.

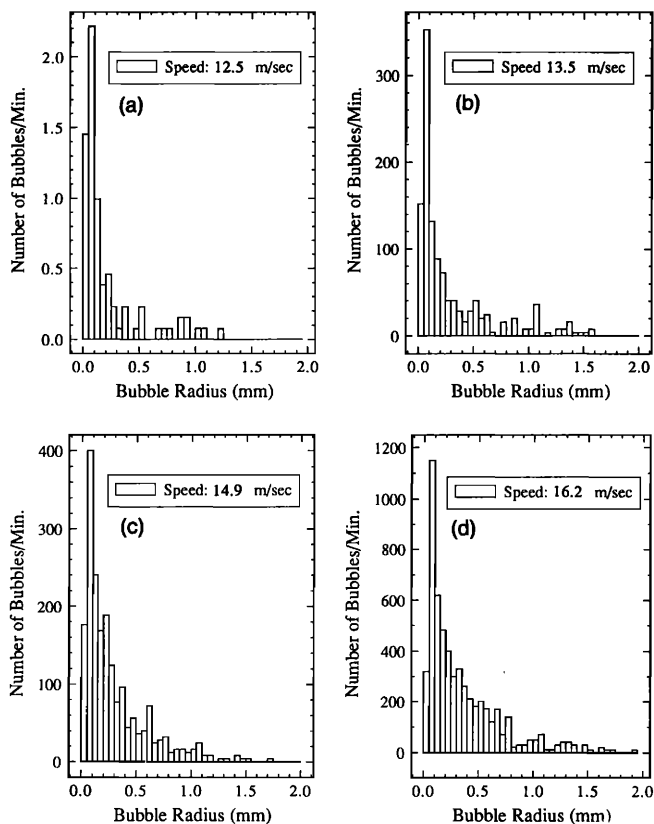


FIG. 12. Power density averaged over 1000 acoustic signals at three different mean wind speeds: 12.5, 13.5, and 16.2 m/s. Also shown is the power density of background noise from the wind generator running at a wind speed of 16.2 m/s and prevented from producing waves. This data was acquired in the large anechoic water tank (12'×12'×8'). The straight line with a slope of 5 dB/oct shows the slope of the Knudsen spectra for ambient noise in the ocean.

16.2 m/s, respectively. These figures show the distribution of bubble sizes less than 2 mm in radius with corresponding frequencies of more than 1.6 kHz.

Using the digital oscilloscope triggered by the output of the preamplifier, discrete acoustic emissions were recorded and bandpassed from 0.80 to 125 kHz using a KH3550 filter, and the corresponding power densities were computed. Figure 12 illustrates the power densities averaged over 1000 recorded emissions with a 20-ms period, which may contain more than one bubble; they were obtained at three different mean wind speeds: (a) 12.5 m/s, (b) 13.5 m/s, and (c) 16.2 m/s. These mean wind speeds were measured in the cross section of the wind tunnel at the entrance to the tank. The background noise of the wind generator was also measured by driving it at a wind speed of 16.2 m/s and preventing it from generating waves. The background noise was averaged over 1000 power densities and is also shown in the same figure. In the anechoic tank the surface tension was approximately 67 dyn/cm. Note the broad range of frequencies (i.e., broad range of generated bubble sizes) centered around 4 kHz. The slopes of the power densities are approximately 5 dB/octave from about 5 to 100 kHz, which is close to the Knudsen wind-generated noise spectra at high frequencies measured in the ocean. The hydrophone location and tank limitation pre-

vented any attempt at making absolute comparisons of sound pressure levels between the tank measurements and Knudsen's results. These curves show a weak dependence on the wind speed. As the wind speed was increased the power spectrum broadened and the peak moved to lower frequencies. This trend confirms our video observations, which show air entrainment includes very small spilling gravity as well as capillary waves at high wind velocities. The high friction velocity may have caused fluid droplets to disengage from the crest of the ripples and may have entrained bubbles.

As the wind speed was increased the bubble size distributions were shifted to larger bubbles [i.e., lower frequencies (Fig. 11)]. This shift can easily be seen in the average power density shown in Fig. 12. The majority of bubble sizes generated by capillary-gravity waves are centered around 0.2 mm in radius, which corresponds to a resonance frequency of approximately 16 kHz. The power densities shown in Fig. 12 show peaks around 4 kHz. The differences in the frequencies and levels of these broadband peaks are attributed to the fact that larger bubbles radiate higher energies than smaller ones and the overall energy of few large bubbles may be greater than a large quantities of smaller bubbles.

### C. Bubble production rate by capillary-gravity waves

Quantitative measurements of bubble production rates for capillary-gravity waves and their relationship to wind speed, surface tension, and laboratory short fetch, measured in the small tank with the coincidence device, are discussed in this section. In the generation of capillary waves, surface tension is the dominant parameter. Conversely, gravity waves are readily excited by elevated wind speeds. It seems reasonable to assume that these factors will influence the rates at which capillary-gravity waves generate bubbles. To test this hypothesis, we measured production rates by counting detected acoustic emissions over a 25-min interval, from which we estimated a rate in bubbles/s. This was repeated five times and the average bubble production rate over the 43-cm<sup>2</sup> area was determined. Figure 13(a)–(d) shows the average bubble production rate/cm<sup>2</sup> versus wind speed for various surface tensions in fresh water as well as in salt water for laboratory fetch distances of 25, 40, 55, and 70 cm, respectively. These figures show that (1) the bubble production rate drastically increases with wind speed, (2) it increases with decreasing surface tension, (3) it decreases with laboratory short fetch, and (4) there is a significant increase in bubble production rate in salt water. The increase in production rate with increasing wind speed is probably because higher wind speeds spawn more energetic gravity-wave activity, which, in turn, leads to more bubble production. This also could be due to the fact that increasing wind speed increases the friction velocity  $u^*$ , which in turn increases the steepness ratio of both capillary and gravity waves. By the same argument, the increase in laboratory fetch distance decreases the frictional velocity, thus entraining fewer bubbles. Figure 13(a)–(d) shows, surprisingly, that lowering the surface tension *raises* the bubble production rate. All of

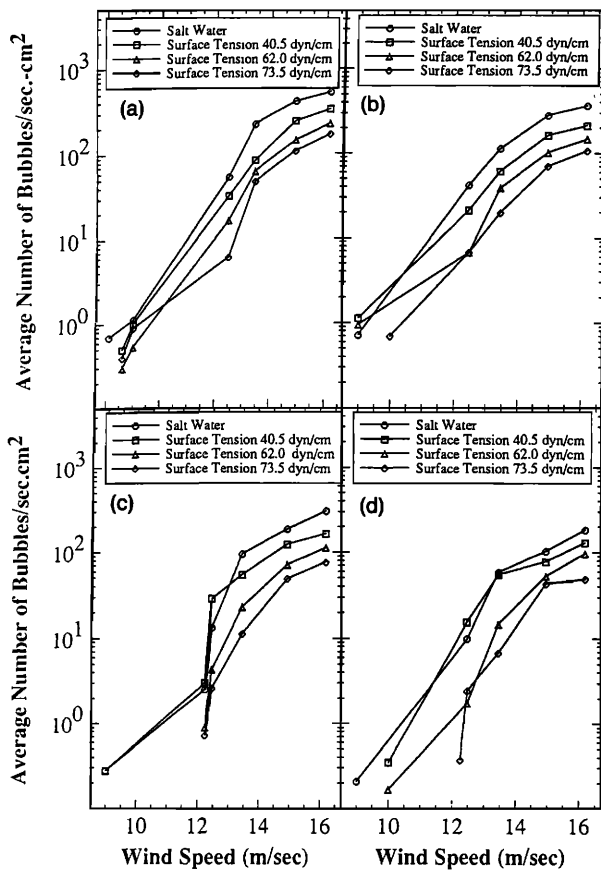


FIG. 13. Mean bubble production rate/s/cm<sup>2</sup> versus mean wind speed in salt water (33 g salt/1000 g water) and fresh water with three different surface tensions: 40.5, 62.0, and 73.5 dyn/cm. (a) fetch=25 cm, (b) fetch=40 cm, (c) fetch=55 cm, and (d) fetch=70 cm. These data are acquired in the smaller tank by utilizing the coincidence detector unit.

these figures indicate a marked increase in bubble production at lower surface tensions. Figure 13(a)–(d) shows the bubble production rate measured over 43 cm<sup>2</sup> in small tank with the coincidence device while Fig. 11(a)–(d) shows the bubble production over the entire area where acoustically active bubble were generated in the anechoic tank. Recent studies of the entrainment of air bubbles by rain drops by Pumphery *et al.*,<sup>27</sup> Scrimger, Evans, and Yee *et al.*,<sup>29</sup> Nystuen,<sup>30</sup> and Rohr and Updegraff<sup>23</sup> indicate that reducing surface tension inhibits entrainment. However, the physical mechanisms governing the production of a bubble by drop impact are much different from that for capillary-gravity wave. In the former, the bubble is produced by the appropriate balance of hydrodynamic and surface forces—reducing the surface tension shifts this balance. In the latter, a reduction in surface tension should lead to an increased tendency to form elongated troughs—less surface energy—and thus increased bubble production rates.

There is evidence of a threshold value for wind speed at approximately 8.6 m/s at a distance 25 cm from the entrance to the tank below which bubble production does not occur. This threshold value remains approximately the same for fresh and salt water, but is slightly decreased to

roughly 8.1 m/s for fresh water at a surface tension of 40.5 dyn/cm.

### III. CONCLUSIONS

We have shown that there is strong evidence that capillary-gravity waves can result in the entrainment of acoustically active bubbles. This is in qualitative agreement with the theoretical works of Crapper,<sup>7</sup> Hogan,<sup>11–14</sup> and Longuet-Higgins.<sup>5</sup> The presence of wind over a free water surface results in the production of capillary-gravity waves, which can, in turn, lead to the generation of a significant number of acoustically active bubbles. Using two synchronized, high-speed video cameras, the causal relationship between capillary wave bubble formation and acoustic emissions was established. It was apparent from video observations that capillary waves can lead to “pinch-off” in the trough, which results in the generation of acoustically active bubbles.

The threshold wind speed for bubble production to occur was measured to be approximately 8.6 m/s at a distance 25 cm from the entrance to the tank (14.6 m/s at 10 m level) for both fresh water and salt water, which is greater than wind force 4 on the Beaufort scale. The mean wind speed threshold value was weakly dependent upon surface tension and was reduced to about 8.1 m/s (13.8 m/s at 10-m level) for a surface tension of 40.5 dyn/cm. The acoustic emissions were monitored for mean wind speeds ranging from 8.4 to 16.2 m/s. The spectral densities of radiated frequencies ranged from a few kilohertz to over 100 kHz, with a broad peak centered around 4 kHz. Video observations indicate that, in addition to the capillary wave gas entrainment mechanism, bubbles are also formed from gas entrained by energetic gravity waves. This effect is demonstrated by the shift in the spectral peaks to lower frequencies as the wind speed increased; along with the shift to lower frequencies, there is a concomitant increase in the average entrained bubble size. The spectral slopes for capillary-gravity waves from several kilohertz to over 100 kHz are approximately 5 dB/octave, which mimic the measured ocean ambient spectrum.<sup>1,2</sup> Capillary wave bubble entrainment is expected to occur over a major portion of the sea surface when the wind speed exceeds the measured threshold value.

Bubble production rates were measured by counting acoustic emissions for different mean wind speeds, surface tensions, and laboratory wind fetches. The bubble production rate is enhanced by increasing wind speeds and is decreased by increasing laboratory short fetch. It is clear that increasing wind speed enhances frictional force on the air–water interface and results in more energetic waves. Increasing laboratory short fetch, which was determined to be inversely proportional to wind speed, reduces the energy transferred from wind to waves. The decrease in the “bulk” surface tension of the water increases the bubble production rate. The exact physical mechanism of an increase in bubble production rates with decreasing surface tension is not yet known. Bubble production rates in salt water are larger by more than a factor of 2 over those in fresh water. The small tank used to study the bubble pro-

duction from capillary-gravity waves was not large enough to generate waves in which some of the parameters (including the fetch) could be scaled to the ocean parameters.

Finally, the acoustic emissions from these bubbles cover a broad frequency range and the bubble production rates are sensitive to environmental conditions such as wind speed, surface tension, and salinity. The relative importance of this effect in the total ambient noise spectra is still to be determined.

## ACKNOWLEDGMENTS

The authors would like to thank Andrea Prosperetti for initiating the project and for providing valuable insight, Joe Burch for automating the system, and Darren Stites and Alex Ruxton for assisting in data acquisition and analysis. This work was supported by the Office of Naval Research.

- <sup>1</sup>V. O. Knudsen, R. S. Alford, and J. W. Emling, "Underwater ambient noise," *J. Mar. Res.* **7**, 410–429 (1948).
- <sup>2</sup>G. M. Wenz, "Acoustic ambient noise in the ocean: spectra and sources," *J. Acoust. Soc. Am.* **34**, 1936–1956 (1962).
- <sup>3</sup>M. S. Longuet-Higgins, "Mechanisms of wave breaking in deep water," in *NATO Advanced Research Workshop on Sound Generation Mechanisms at the Ocean Surface*, Lerici, Italy (NATO, Geneva, 1987).
- <sup>4</sup>C. S. Cox, "Measurements of slopes of high-frequency wind waves," *J. Mar. Res.* **16**, 199–225 (1958).
- <sup>5</sup>M. S. Longuet-Higgins, "The generation of capillary waves by steep gravity waves," *J. Fluid Mech.* **16**, 138–159 (1963).
- <sup>6</sup>James Lighthill, *Waves in Fluids* (Cambridge U.P., London, 1975).
- <sup>7</sup>G. D. Crapper, "An exact solution for progressive capillary of arbitrary amplitude," *J. Fluid Mech.* **2**, 532–539 (1957).
- <sup>8</sup>A. H. Schooley, "Profiles of wind-generated water waves in the capillary-gravity transition region," *J. Mar. Res.* **16**, 100–108 (1958).
- <sup>9</sup>A. H. Schooley, "Double, triple, and higher-order dimples in the profiles of wind-generated water waves in the capillary-gravity transition region," *J. Geophys. Res.* **65**, 4075–4079 (1960).
- <sup>10</sup>J. R. Wilton, "On ripples," *Philos. Mag.* **29**, 688–700 (1915).
- <sup>11</sup>S. J. Hogan, "Some effects of surface tension on steep water waves, Part 1," *J. Fluid Mech.* **91**, 532–540 (1979).
- <sup>12</sup>S. J. Hogan, "Some effects of surface tension on steep water waves, Part 2," *J. Fluid Mech.* **96**, 417–445 (1980).
- <sup>13</sup>S. J. Hogan, "Some effects of surface tension on steep water waves, Part 3," *J. Fluid Mech.* **110**, 4381–410 (1981).
- <sup>14</sup>S. J. Hogan, "Surface tension effects in nonlinear waves," in *Oceanic Whitecaps*, edited by E. C. Monahan and G. MacNiocaill (Reidel, Dordrecht, 1986), pp. 147–158.
- <sup>15</sup>R. L. Miller, Tech. Rep. No. 13, The University of Chicago, Fluid Dynamics and Sediment Transport Laboratory, Dept. of Geophysical Sciences (1972).
- <sup>16</sup>G. E. Updegraff and V. C. Anderson, "An instrument for the *in situ* measurement of sea surface noise from a depth of 1 m under low wind conditions," *J. Acoust. Soc. Am.* **89**, 2253–2263 (1991).
- <sup>17</sup>G. E. Updegraff and V. C. Anderson, "Bubble noise and wavelet spills recorded 1 m below the ocean surface," *J. Acoust. Soc. Am.* **89**, 2264–2279 (1991).
- <sup>18</sup>H. Medwin and M. M. Beaky, "Bubble sources of the Knudsen sea noise spectra," *J. Acoust. Soc. Am.* **86**, 1124–1130 (1989).
- <sup>19</sup>J. H. Wilson, "Wind-generated noise modeling," *J. Acoust. Soc. Am.* **73**, 211–216 (1983).
- <sup>20</sup>B. R. Kerman, "Underwater sound generation by breaking waves," *J. Acoust. Soc. Am.* **75**, 149–165 (1984).
- <sup>21</sup>J. Rohr, R. Glass, and B. Castile, "Effect of monomolecular films on the underlying ocean ambient-noise field," *J. Acoust. Soc. Am.* **85**, 1148–1157 (1989).
- <sup>22</sup>J. Rohr and R. Detsch, "A low sea-state study of the quieting effect of monomolecular films on the underlying ambient-noise field," *J. Acoust. Soc. Am.* **92**, 365–382 (1992).
- <sup>23</sup>J. Rohr and G. Updegraff, "The effect of monomolecular films on low sea state ambient noise," in *Natural Physical Sources of Underwater Sound*, edited by B. Kerman (Kluwer Academic, Boston, MA, 1993).
- <sup>24</sup>Y. Toba "Drop production by bursting of air bubbles on the sea surface (III)—study by use of wind flume," *Mem. Coll. Sci. Univ. Kyoto Ser. A XXIX* (3), Article 4, 313–344 (1960).
- <sup>25</sup>H. Mitsuyasu, "Measurement of the high-frequency spectrum of ocean surface waves," *J. Phys. Oceanogr.* **7**, 882–891 (1977).
- <sup>26</sup>M. S. Longuet-Higgins, B. R. Kerman, and K. Lunde, "The release of air bubbles from an underwater nozzle," *J. Fluid Mech.* **230**, 365–390 (1991).
- <sup>27</sup>H. C. Pumphery, L. A. Crum, and L. Bjørnø, "Underwater sound produced by individual drop impacts and rainfall," *J. Acoust. Soc. Am.* **85**, 1518–1526 (1989).
- <sup>28</sup>M. Minnaert, "On musical air-bubbles and the sounds of running water," *Philos. Mag.* **16**, 235–248 (1933).
- <sup>29</sup>J. A. Scrimger, D. J. Evans, and W. Yee, "Underwater noise due to rain—open ocean measurements," *J. Acoust. Soc. Am.* **85**, 726–731 (1989).
- <sup>30</sup>J. A. Nystuen, "Rainfall measurements using underwater ambient noise," *J. Acoust. Soc. Am.* **79**, 972–982 (1986).